Concurrent Session 2

DNA Damage, Repair and Genome Stability

Characterization of Two H2AX Homologues in *Arabidopsis thaliana* and their Response to Ionizing Radiation

N D Huefner[1,*], J D. Friesner[2] & A B Britt[1]

Abstract

Phosphorylation of histone variant H2AX at the site of DNA double-strand breaks (DSB) is one of the earliest responses detected in cells exposed to Ionizing Radiation (IR). Phosphorylated H2AX (γ-H2AX) is important for recruiting and retaining repair proteins at the site of DSBs and contributes to the maintenance of cell-cycle arrest until repair is completed. In this study, insertional mutants of two *Arabidopsis thaliana* H2AX homologues were identified and characterized to determine if both genes are functionally active and whether their roles are redundant or divergent. We report an approximate ten-fold reduction in γ-H2AX in our double mutant line and demonstrate that the homologues function redundantly in the formation of IR induced γ-H2AX foci. A tendency towards increased inhibition of root growth was observed in irradiated double mutant plants relative to both wild-type and single mutant lines. No evidence indicating a functional divergence between the two homologues was detected.

Introduction

Protection against genomic instability is of major importance to all organisms. Failure to rapidly identify or appropriately respond to DNA damage can lead to deletions, chromosomal rearrangement, and loss of heterozygosity; such changes are frequently deleterious and potentially lethal. DNA double-strand breaks (DSBs), both of intrinsic and extrinsic origin, constitute one significant source of genomic instability. Metabolic byproducts [1, 2], ionizing radiation (IR) [3, 4], radiomimetic compounds [4-6], and meiosis [7] are all known to generate DSBs. Given the fundamental importance of a timely and reliable response to DSBs, it is not surprising that a high degree of homology exists between DSB recognition and repair pathways in yeasts, plants, and animals [8, 9].

One of the earliest observed responses to induction of DSBs is phosphorylation of the histone variant H2AX by the PIK-related protein kinase (PIKK) family member ataxia telangiectasia mutated (ATM) and to a lesser extent by **a**taxia **t**elangiectasia mutated and **r**ad3-related (ATR) [10-12]. This histone variant, characterized by a terminal SQE motif, is phosphorylated within minutes of induction of a DSB [13]. Phosphorylation of H2AX at the site of a DSB is thought to be important in retaining and concentrating repair proteins at the site of the break [14-16]. Evidence indicates that phosphorylated H2AX, termed γ-H2AX [17], also plays a role in recruiting chromatin modifiers to the lesion to facilitate repair [18]. Following repair, dephosphorylation of γ-H2AX is important for the cell to resume cycling [19, 20].

H2AX is highly conserved among eukaryotes [21]. Two putative H2AX protein homologues were identified in the model plant *Arabidopsis thaliana* [10]. These homologues, termed *H2AXa* (GenBank locus At1g08880) and *H2AXb* (GenBank locus At1g54690) are predicted to differ at only two of 142 amino acids. Here we demonstrate that *atH2AXa* and *atH2AXb* function redundantly in the formation of IR induced γ-H2AX foci; no divergent roles for the two homologues were observed.

[1] Section of Plant Biology, University of California-Davis, Davis, CA 95616, USA
[2] Section of Molecular and Cellular Biology, University of California -Davis

* Corresponding author. E-mail: ndhuefner@ucdavis.edu

Materials and Methods

Isolation of Mutants

Arabidopsis thaliana T-DNA insertion mutants of *atH2AXa* (At1g54690) and *atH2AXb* (At1g54690) were obtained from the SAIL collection ('SALK_007006.29.20.x', and 'SALK_012255.55.25.x' respectively) through the ABRC. The T-DNA-specific primer used in the isolation of both mutants was 'LBa1' (5'-TGGTTCACGTAGTGGGCCATCG-3'). The gene-specific primer used in the detection of atH2AXa was 'AL1' (5'-GCTCCATGAGTTGCATGTATCTGC-3'). The gene-specific primer used in the detection of *atH2AXb* was 'BL2' (5'-CTCTTCATCGTTCCTCACTGCAAG-3'). The T-DNA insertion site of *atH2AXa* was sequenced using primers 'LBa1' and 'AL1' for one left border and 'LBa1' and 'AU1' (5'-TCGATCAACCCTGGCCATCTT-3') for the second left border. Primers 'LBa1' and 'BL2' were used to sequence the left border T-DNA integration site in *atH2AXb*. Gene-specific primers 'AL2' (5'-ACGTGTCTTCTTGTTATCCCTTGC-3') and 'AU2' (5'-CCTAAAGCCCACTCATCTTC-3') were used to detect the wild-type allele of *atH2AXa*. Gene-specific primers 'BL1' (5'- CTCTTGAGAAGCAGATCCGATATCGC-3') and 'BU1' (5'-CCGCGTGACTCACAACTAACCAAT-3') were used to detect the wild-type allele of *atH2AXb*.

Plant Material and Growth Conditions

Plants used in this study were of a *Col* background. Plants used for protein extraction were grown on Premier Pro soil mix (Premier Horticulture, Quebec, Canada). Seeds to be used for root tip excisions and for root growth measurements were surface sterilized for 10 minutes in a solution of 20% bleach and 0.2% Tween, and then rinsed 10 times in ddH2O. Sterilized seeds were sown on nutritive MS-agar plates and stored at 4°C for three days before being transferred to normal growing conditions. Plates were placed in a vertical orientation so that roots would grow along the surface of the agar. Plants were grown at 20°C and 60% humidity in ConvironcmP4040 growth chambers. A 16 h day/8 h night cycle was simulated using light from cool-white lamps (100-150 μmol m^{-2} s^{-1}) filtered through Mylar.

Gamma Irradiations

A Cs137 source (Institute of Toxicology and Environmental Health, University of California, Davis) was used to irradiate seeds at a dose rate of 6.9Gy sec^{-1}. Plants used for protein extraction were irradiated with 100 or 200Gy IR or mock-treated 14 days after planting (DAP). Above ground tissue was harvested into liquid nitrogen 15 minutes after treatment and stored at -80°C until the time of protein extraction. Seedlings used in root tip excisions were irradiated with five or 2.5Gy IR or mock-treated 5 DAP; samples were fixed in paraformaldehyde five minutes

after treatment and the root tips excised as described below. Seedlings used in root growth assays were irradiated with indicated doses 5 DAP.

Protein Extractions and Immunoblots

Histones were harvested as described previously [22]. Sodium fluoride (Sigma, St. Louis, MO) and sodium ortho-vanadate (Sigma) were used at final concentrations of 30 mM and 100 μM respectively to inhibit dephosphorylation of proteins. Extracts were quantified using the Bradford assay and prepped for immunoblotting as previously reported [10]. Protein samples were separated on a 12.5% polyacrylamide gel and then transferred to nitrocellulose membranes over a period of four hours at 4°C in 20% methanol transfer buffer under a constant current of 400 mA. Blots were stained for five minutes in Ponceau S (P-3504, Sigma) solution to qualitatively evaluate protein loading and transfer. Blots were destained and transferred to a solution of 2% nonfat dry milk in 1x Tris-buffered saline (TBS)-T (0.05% final concentration Tween-20) where they incubated on an orbital shaker for one to three hours at room temperature. Blots were then incubated in rabbit antiplant γ-H2AX primary antibody [10] diluted in 2% nonfat milk in 1x TBS-T on a rocking platform for 2h at room temperature. Blots were rinsed twice in ddH_2O and once in 1x TBS-T (five minutes each time) on an orbital shaker, before transfer to a solution of anti-rabbit immunoglobulin horseradish peroxidase-linked secondary antibody (Amersham Biosciences NA934V, Piscataway, NJ) diluted 1:10,000 in 2% nonfat milk in 1x TBS-T. Blots were incubated in secondary antibody on an orbital shaker at room temperature for 1-1.5h, at which point they were rinsed with ddH2O and 1x TBS-T as above. Blots were then treated with enhanced chemiluminescence reagents (ECL Plus) as described (RPN 2131, Amersham Biosciences) and exposed to X-ray film (CL-XPosure film, Pierce, Rockland, IL).

Quantification of Relative -H2AX Content

To estimate γ-H2AX content in our mutant lines relative to wild-type, fresh protein extractions were made from plants irradiated with a dose of 200Gy as described above. 15.0 ng of extracted protein from *ath2axa, ath2axb,* and *ath2axa;ath2axb* were loaded on a polyacrylamide gel. A dilution series of WT protein extract was also loaded on the gel (2x, 1x, 0.25x, and 0.0625x where 1x=15ng). Separation, transfer, and immunoblotting of γ-H2AX was carried out as described above. To increase the sensitivity of the x-ray film and to increase the linear range of detection, film was pre-exposed using an automatic flash (Sunpak Softlite 1600A, ToCAD, Rockaway, NJ) masked with porous paper. An optimal exposure distance of 50cm was empirically determined such that a pre-exposure flash increased the 540 nm absorbance of pre-exposed film by 0.15 with respect to film that had not been pre-exposed [23, 24]. Pre-exposed film was immediately used to detect chemiluminescent signal from the immunoblots. Developed images were digitally scanned (Epson Perfection 2400 Photo, Epson, Long Beach, CA), and analyzed using 'ImageQuant™ v5.2' (GE Healthcare, Piscataway, NJ). Total signal for each band was calculated as the integrated intensity of all pixels within a user defined box that encompassed that band. A local average correction for each band was used to exclude background signal. The adjusted signal for the wild-type dilution series was used to generate a standard curve of signal intensity vs. relative γ-H2AX content in 15 ng of protein extract. This curve was used to estimate the γ-H2AX content of our mutant lines relative to wild-type.

Root Tip Excision, Slide Preparation, and Immunostaining

Root tips were excised and mounted as described [25] with the modifications reported [10]. Slides were stored at -80°C until they were ready to be stained and scored. Root tip nuclei were stained to visualize γ-H2AX, tubulin, and chromosomal DNA as described [10]. After an overnight incubation at 4°C, nuclei were visualized, scored, and images captured [10].

Root Growth Assay

Seeds used in root growth assays were prepared and irradiated or mock-irradiated as described above. An image of each plate was captured immediately after irradiation, 0 days after treatment (DAT), using a CoolSNAP CCD camera (Photometrics, Tucson, AZ) affixed to a Zeiss Stemi SV 11 stereomicroscope (Zeiss, Thornwood, NY); plates were then returned to the growth chamber. A second image of each plate was captured 7 DAT. Root lengths were determined by tracing the primary root using the image processing and analysis software 'ImageJ' [26]. To reduce error introduced by seeds that did not germinate, seeds that germinated late, and seedlings whose roots did not achieve or maintain good contact with the vertical agar surface, only those plants whose primary root length was in at least the plate's 66th percentile 0 DAT were included in the data set. Root length 0 DAT was subtracted from root length 7 DAT to obtain post-treatment root growth (PTRG). PTRG of irradiated plants was normalized to PTRG of mock-treated lines.

Results

Isolation of *atH2AXa* and *atH2AXb* insertion mutants

The publicly available seed stocks of the Arabidopsis Biological Resource Center (ABRC) were screened to identify possible insertional mutants in *atH2AXa* and *atH2AXb*. Annotated sequence information from the Salk Institute Genomic Analysis Laboratory (SAIL) identified two potentially valuable lines: ABRC line 'SALK_007006.29.20.x', whose transferred DNA (T-DNA) mapped somewhere near the first exon of *atH2AXa*, and ABRC line 'SALK_012255.55.25.x', whose T-DNA mapped to the middle of *atH2AXb*. Polymerase chain reaction (PCR) primers were designed according to the DNA sequences found in the SAIL database and used to verify the presence of the T-DNA in each line. The insertion site of each line was characterized by sequencing off of the T-DNA border sequence. Sequencing of the insertion site of 'SALK_007006.29.20.x' (*ath2axa*) indicated that the T-DNA is located 68 bp upstream of the start codon of *atH2AXa*. The insertion is accompanied by a deletion of 8 bp and, based on PCR and sequencing data, has two left borders pointing away from the insertion site into the genomic DNA (**Fig. 1a**). Characterization of the insertion site of 'SALK_012255.55.25.x' (*ath2axb*) proved to be more difficult as we were only able to obtain PCR and sequencing data from one border of the T-DNA insert. Sequencing off the left border indicated that the T-DNA is located in *atH2AXb'* s only intron, 84 bp upstream of the second exon (**Fig. 1b**). While we were unable to obtain PCR products or sequencing information from the other border using both left and right border sequence information, genomic primers spanning *atH2AXb'* s coding sequence gave no product in lines homozygous for the T-DNA insert; those same primer combinations give clear bands in heterozygous *atH2AXb* and wild-type lines, suggesting that the T-DNA insert truly does disrupt the wild-type copy of *atH2AXb* rather than simply duplicating a portion of the gene and reinserting elsewhere in the genome, leaving a wild-type copy of the gene intact.

Figure 1 Gene structure and T-DNA insertion site of mutant lines *ath2axa* **(a)** and *ath2axb* **(b)**. Shaded line, UTR; black line, intron; black box, exon; gap, 8 bp deletion; triangle, T-DNA; LB, T-DNA left border; regular text, genomic DNA sequence; underlined text, T-DNA border sequence; parenthetical text, DNA sequence that matches neither T-DNA border sequence nor genomic DNA exactly; ellipsis, continuation of adjacent DNA sequence; question mark, unresolved T-DNA border and insertion site.

After confirming the locations of the T-DNAs, lines *ath2axa* and *ath2axb* were crossed and their F_2 progeny screened to identify homozygous lines. Using a T-DNA left border specific primer and flanking gene specific primers we were able to isolate homozygous double mutant *ath2axa;ath2axb* lines as well as recover homozygous single mutant lines for both *ath2axa* and *ath2axb*. Wild-type segregants were also identified and maintained for use as controls in subsequent experiments. The mutant lines isolated were both viable and fertile. No morphological difference was apparent in either single mutant or double mutant plants. Genetic crosses using *ath2axa, ath2axb*, or *ath2axa;ath2axb* were successful in all cases, regardless of whether the mutant line functioned as the maternal source (ovule), the paternal source (pollen), or both (self-cross).

Production of γ-H2AX is repressed in H2AX mutants.

To test if *ath2axa* and *ath2axb* are still capable of producing functional H2AX protein, histones from homozygous lines were extracted before and after exposure to IR and probed with polyclonal *Arabidopsis* γ-H2AX antibodies [10]. In extracts from wild-type plants taken 15 minutes after exposure to 200Gy gamma radiation, a clear band of ~16 kDa is observed, reflecting the presence of IR induced γ-H2AX protein; comparable bands are detected in extracts from IR treated single mutant *ath2axa* and *ath2axb* plants. In extracts from IR treated double mutant *ath2axa;ath2axb* plants, the ~16kDa band is faint, though discernable, suggesting that at least one of the mutant lines is not a complete loss of function mutation (**Fig. 2a**). Control experiments, in which extract from IR treated double mutant *ath2axa;ath2axb* plants was run separately from other positive lanes, indicate that faint γ-H2AX signal detected is not the result of spillover from adjacent lanes. By comparing the signal intensity of the γ-H2AX band observed in the single and double mutant H2AX lines to that of a wild-type dilution series (**Fig. 2b**), we estimate an approximate ten-fold reduction in γ-H2AX content for *ath2axa;ath2axb* plants relative to wild-type plants (**Fig. 2c**).

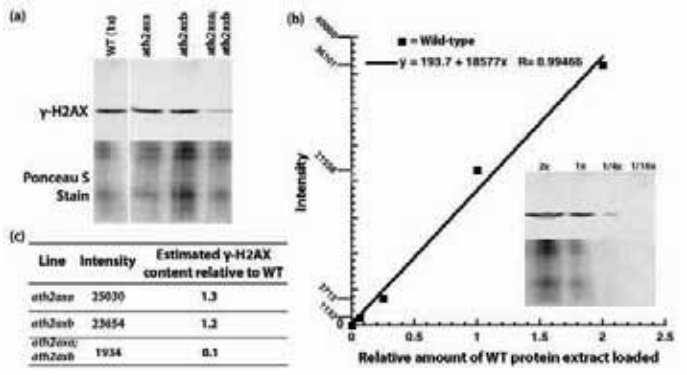

Figure 2 Quantification of γ-H2AX in wild-type and mutant lines. Plants were irradiated with 200Gy gamma radiation and harvested 15 minutes after removal from source. Ponceau S staining was carried out prior to immunoblotting as a qualitative control for protein loading and uniformity of transfer. **(a)** Assessment of γ-H2AX induction in response to IR in wild-type and mutant lines by immunoblot. Image is representative of blots from four experiments. **(b)** Linear regression of immunoblot γ-H2AX band intensity, corrected for local average background signal, as a function of relative amount of wild-type (WT) protein extract loaded. The amount of sample loaded ranged from 2x to 1/16x (inset), where 1x is equivalent to 15 ng of protein extract. **(c)** Estimate of γ-H2AX content in mutant lines relative to wild-type as determined from (b).

Neither single mutant exhibited decreased levels of γ-H2AX content relative to wild-type. A faint ~16 kDa band is also observed in extracts from untreated wild-type, untreated *ath2axa*, and untreated ath2axb plants; this band is not detected in untreated *ath2axa;ath2axb* plants (data not shown). Presence of this band in extracts from untreated wild-type plants has been previously reported and may reflect some low, steady state level of phosphorylation in cells, or may be due to low level detection of unphosphorylated H2AX by the polyclonal antibodies [10].

H2AXa and H2AXb act redundantly in the formation of IR induced γ-H2AX

While it is clear from our immunoblot experiments that both H2AXa and H2AXb are phosphorylated in response to IR, it was unclear whether the two proteins function redundantly in the formation of the γ-H2AX foci characteristic of DSB response. To address this question, γ-H2AX foci were quantified in *ath2axa, ath2axb*, and *ath2axa;ath2axb* root tips exposed to IR. Only a slight difference in the number of foci produced per Gy gigabasepair (Gy*Gbp) was observed in either single mutant (**Fig. 3**). This suggests that H2AXa and H2AXb function redundantly in the establishment of IR induced foci. Consistent with this hypothesis is the fact that we were unable to detect production of γ-H2AX foci in our *ath2axa;ath2axb* double mutant plants. Of the 74 mitotic root tip cells scored, no γ-H2AX foci were observed, suggesting that a wild-type copy of either of these two homologues is essential for the formation of γ-H2AX foci. While our immunoblot results indicate the presence of some γ-H2AX in our IR treated *ath2axa;ath2axb* double mutant line, any contribution it may make to the formation of foci is below our level of detection.

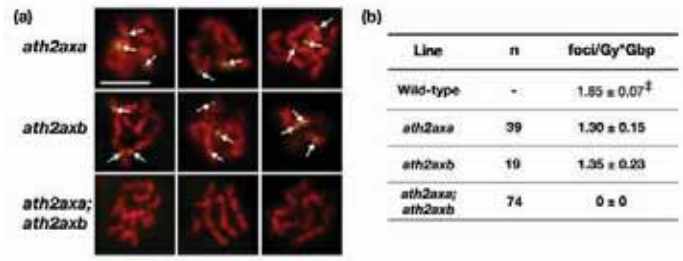

Figure 3 γ-H2AX foci formation in atH2AX mutant lines. **(a)** Immunoflourescence of mutant root tip nuclei irradiated with 5Gy gamma radiation. γ-H2AX foci (green) are overlayed onto chromosomes (red) stained with DAPI. Arrows highlight positions of γ-H2AX foci. Scale bar, 5 μm. **(b)** Number of γ-H2AX foci generated per Gy per gigabasepair (Gbp) ± standard error. Root tip nuclei were irradiated with either 5Gy or 2.5Gy gamma radiation. n, number of root tip nuclei scored. ‡, rate of foci induction in wild-type root tip nuclei exposed to 5Gy or 2.5Gy gamma was calculated from previous experimental data (Friesner, 2005).

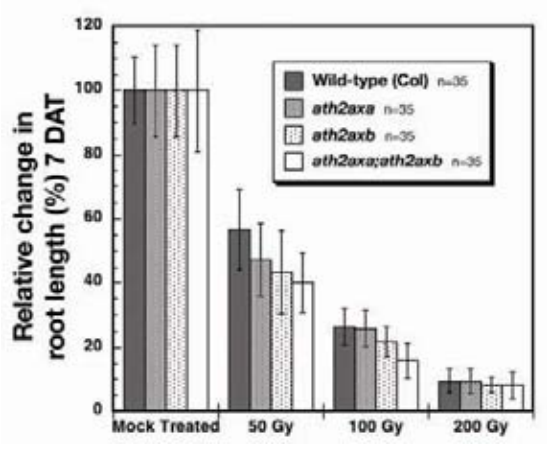

Figure 4 Root growth of IR treated lines in the first seven days after gamma treatment (7 DAT). Values expressed as percent change in root length relative to percent change in root length of mock treated plants. Error bars, standard error; n, number of plants scored.

A subtle change in root growth following exposure to gamma radiation is observed in H2AX mutants.

We sought to further investigate the importance of H2AXa and H2AXb in response to gamma radiation by assaying root growth in each of our mutant lines. Monitoring root growth, a product of both cell division and cell expansion, is a simple means of quantifying the impact of DNA damaging agents on a plant. In the days immediately following exposure to gamma radiation, the wild-type line, both single mutant H2AX lines, and the double mutant line all displayed decreases in overall root growth correlated to the dose of IR they received (**Fig. 4**).

Our single mutant lines *ath2axa* and *ath2axb* both displayed a slightly greater inhibition of root growth than wild-type, though the difference was not statistically significant. In our IR treated double mutant seedlings, an even greater inhibition of root growth was observed, though the difference relative to wild-type was still not statistically significant. This trend is observed across a range of IR doses, though it is most obvious at a dose of 100Gy . While the effect of gamma radiation on root growth is not significantly different between wild-type and mutant lines, the overall trend suggests that the two *Arabidopsis* H2AX homologues play redundant roles in the plant's response to DSBs.

Discussion

H2AXa and H2AXb may act redundantly in the response of *Arabidopsis thaliana* to ionizing radiation.

In this article we report the identification and isolation of a pair of T-DNA insertional mutants affecting the expression of two H2AX homologues, *atH2AXa* and *atH2AXb*, encoded by the model plant *Arabidopsis thaliana*. Although we were unable to obtain a line in which H2AX production is completely abolished, we demonstrate a roughly ten-fold reduction in the amount of γ-H2AX produced in response to gamma radiation in our double mutant line. Given that untreated *atH2AXa*, *atH2AXb*, and *atH2AXa;atH2AXb* plants exhibit no obvious changes in either their overall morphology or their growth habits, it is clear that wild-type levels of H2AX are not essential for viability in *A.thaliana*. While it is possible that a full loss of function line would be inviable, our results are consistent with the observation that H2AX-deficient mouse embryonic stem cells are also viable [27]. Unlike H2AX-deficient mice, however, which display a significant reduction in fertility [28], no defect in fertility was observed in *atH2AXa;atH2AXb* plants; this may indicate that very low levels of H2AX are sufficient to carry out meiotic processes during gametogenesis. Alternatively, H2AX may be wholly unnecessary in *A. thaliana* for normal meiotic recombination and fertility.

While H2AX may not be essential for cell viability, it does play an important role in resistance to DSB inducing agents [13, 27]. The role of γ-H2AX in IR resistance in plants has not yet been determined. We demonstrate that *atH2AXa* and *atH2AXb* function redundantly in IR induced γ-H2AX foci formation, an early and rapid step in a cell's response to DSBs. We report a slight decrease in root growth following exposure to IR in our double mutant line relative to wild-type, suggesting *atH2AXa* and *atH2AXb* may play a role in mitigating the effects of damage caused by IR. Whether the minor decrease in root growth we observe is due to the persistence of unresolved damage, reflects a defect in the ability of cells to resume normal cycling, or is a result of some other defect is unknown. It is clear from our results that *atH2AXa* and *atH2AXb* act redundantly in the overall production of γ-H2AX in irradiated seedlings and in focus formation in irradiated root tips of *A.thaliana*; however, this does not preclude the possibility that divergent functions may also exist that distinguish the two homologues. The precise role H2AX plays in DNA damage response and cell cycling, and more specifically, the roles *atH2AXa* and *atH2AXb* play in *A.thaliana*, remain open and warrant further investigation.

ACKNOWLEDGEMENTS

We thank Dr. Bo Liu and Dr. Ken Kaplan for their kind assistance and the Salk Institute for the sequence-indexed T-DNA insertion mutants. This work was funded by an NIH training grant (# T32 GM070377), an Elsie Stocking Memorial Fellowship, and from the National Research Initiative of the USDA Cooperative State Research, Education and Extension Service (#04-35301-14740).

BIBLIOGRAPHY

1. Ragu, S. *et al.* Oxygen metabolism and reactive oxygen species cause chromosomal rearrangements and cell death, *Proc. Natl. Acad. Sci. Usa* **104**(23), 9747-9752 (2007).
2. Barnes, D.E. DNA damage: Air-Breaks? *Curr. Biol.* **12**(7), R262-264 (2002).
3. Sutherland, B.M., Bennett, P.V., Sidorkina, O., Laval, J. Clustered DNA damages induced in isolated DNA and in human cells by low doses of ionizing radiation. *Proc. Natl. Acad. Sci. Usa* **97**(1), 103-108 (2000).
4. Regulus, P., *et al.* Oxidation of the sugar moiety of DNA by ionizing radiation or bleomycin could induce the formation of a cluster DNA lesion. *Proc. Natl. Acad. Sci. Usa* **104**(35), 14032-14037 (2007).
5. Degrassi, F., Fiore, M., Palitti, F. Chromosomal aberrations and genomic instability induced by topoisomerase-targeted antitumour drugs. *Curr. Med. Chem. Anti Canc. Agents* **4**(4), 317-325 (2004).
6. Povirk, L.F. DNA damage and mutagenesis by radiomimetic DNA-cleaving agents: bleomycin, neocarzinostatin and other enediynes. *Mutat. Res.* **355**(1-2), 71-89 (1996).
7. Keeney, S., Neale, M.J. Initiation of meiotic recombination by formation of DNA double-strand breaks: mechanism and regulation. *Biochem. Soc. Trans.* **34**(Pt 4), 523-525 (2006).
8. Melo, J., Toczyski, D. A. A unified view of the DNA-damage checkpoint. *Curr. Opin. Cell Biol.* **14**(2), 237-245 (2002).
9. Bleuyard, J.Y., Gallego, M.E., White, C.I. Recent advances in understanding of the DNA double-strand break repair machinery of plants. *DNA Repair (Amst.)* **5**(1), 1-12 (2006).
10. Friesner, J.D., Liu, B., Culligan, K., Britt, A.B. Ionizing radiation-dependent gamma-H2AX focus formation requires ataxia telangiectasia mutated and ataxia telangiectasia mutated and Rad3-related. *Mol. Biol. Cell.* **16**(5), 2566-2576 (2005).
11. Burma, S., Chen, B.P., Murphy, M., Kurimasa, A., Chen, D.J. ATM phosphorylates histone H2AX in response to DNA double-strand breaks. *J. Biol. Chem.* **276**(45), 42462-42467 (2001).
12. Ward, I.M., Chen, J. Histone H2AX is phosphorylated in an ATR-dependent manner in response to replicational stress. *J. Biol. Chem.* **276**(51), 47759-47762 (2001).
13. Downs, J.A., Lowndes, N.F., Jackson, S.P. A role for *Saccharomyces cerevisiae* histone H2A in DNA repair. *Nature* **408**(6815), 1001-1004 (2000).
14. Celeste, A. *et al.* Histone H2AX phosphorylation is dispensable for the initial recognition of DNA breaks. *Nat. Cell. Biol.* **5**(7), 675-679 (2003).
15. Chen, X. Arciero, C.A., Wang, C., Broccoli, D., Godwin, A.K. BRCC36 is essential for ionizing radiation-induced BRCA1 phosphorylation and nuclear foci formation. *Cancer Res.* **66**(10), 5039-5046 (2006).
16. Paull, T.T. *et al.* A critical role for histone H2AX in recruitment of repair factors to nuclear foci after DNA damage. *Curr. Biol.* **10**(15), 886-895 (2000).
17. Rogakou, E.P., Pilch, D.R., Orr, A.H., Ivanova, V.S., Bonner, W.M. DNA double-stranded breaks induce histone H2AX phosphorylation on serine 139. *J. Biol. Chem.* **273**(10), 5858-5868 (1998).
18. Fillingham, J., Keogh, M.C., Krogan, N.J. GammaH2AX and its role in DNA double-strand break repair. *Biochem. Cell Biol.* **84**(4), 568-577 (2006).
19. Downey, M., Durocher, D. GammaH2AX as a checkpoint maintenance signal. *Cell Cycle* **5**(13), 1376-1381 (2006).
20. Nakada, S., Chen, G.I., Gingras, A.C., Durocher, D. PP4 is a gammaH2AX phosphatase required for recovery from the DNA damage checkpoint. *Embo Rep.* (2008).
21. Redon, C. *et al.* Histone H2A variants H2AX and H2AZ. *Curr. Opin. Genet. Dev.* **12**(2), 162-169 (2002).
22. Jackson, J.P. *et al.* Dimethylation of histone H3 lysine 9 is a critical mark for DNA methylation and gene silencing in *Arabidopsis thaliana*. *Chromosoma* **112**(6), 308-315 (2004).
23. Laskey, R.A., Mills, A.D. Quantitative film detection of 3H and 14C in polyacrylamide gels by fluorography. *Eur. J. Biochem.* **56**(2), 335-341 (1975).

24. Voytas, D., Ke, N. Detection and quantitation of radiolabeled proteins in gels and blots. *Curr. Protoc. Cell. Biol.* **Chapter 6**, Unit 6.3 (2001).

25. Liu, B., Marc, J., Joshi, H.C., Palevitz, B.A. A gamma-tubulin-related protein associated with the microtubule arrays of higher plants in a cell cycle-dependent manner. *J. Cell. Sci.* **104** (Pt 4), 1217-1228 (1993).

26. Abramoff, M.D., Magelhaes, P.J., Ram, S.J. Image Procession with ImageJ. *Biophotonics Int.* **11**(7), 36-42 (2004).

27. Bassing, C.H. *et al.* Increased ionizing radiation sensitivity and genomic instability in the absence of histone H2AX. *Proc. Natl. Acad. Sci. Usa* **99**(12), 8173-8178 (2002).

28. Celeste, A. *et al.* Genomic instability in mice lacking histone H2AX. *Science* **296**(5569), 922-927 (2002).

Role of Human Disease Genes for the Maintenance of Genome Stability in Plants

H Puchta*, D Kobbe, K Wanieck, A Knoll, S Suer, M Focke & F Hartung

Abstract

In the plant genome a row of homologs of human genes can be found that, if mutated, are correlated with a high incidence of cancer in humans. Here we describe our recent results on homologs of the breast cancer genes BRCA1/BARD1 and RecQ helicase homologs in the model plant *Arabidopsis thaliana*. HsBRCA1 and HsBARD1 are tumor suppressor proteins that are involved in many cellular processes, such as DNA repair. Loss of one or the other protein results in early embryonic lethality and chromosomal instability. The Arabidopsis genome harbors one BRCA1 homolog, and we were able to identify a BARD1 homolog as well. AtBRCA1 and AtBARD1 are able to interact with each other as indicated by *in vitro* and *in planta* experiments. Our analyses of T-DNA insertion mutants for both genes, revealed that in plants, in contrast to animals, these genes are dispensable for development or meiosis. Nevertheless, we could show that AtBARD1 plays a prominent role in the regulation of homologous DNA repair in somatic cells. RecQ helicases are known as mediators of genome stability. The loss of RecQ function is often accompanied by hyperrecombination due to a lack of crossover suppression. *Arabidopsis thaliana* possesses seven different RecQ genes. We could show that two of them (*AtRECQ4A* and *AtRECQ4B*) arose as a result of a recent duplication and are still 70% identical on protein level. Disruption of these genes, surprisingly, leads to antagonistic phenotypes: the *AtRECQ4A* mutant shows sensitivity to DNA damaging agents, enhanced homologous recombination and lethality in an *Atmus81* background. Moreover, mutation of *AtRECQ4A* partially suppresses the lethal phenotype of an *AtTOP3a* mutant. In contrast, the *AtRECQ4B* mutant shows a reduced level of HR and none of the other phenotypes described above. Finally, we have started to characterize the different RecQ proteins of Arabidopsis by biochemical means and present here the results on AtRECQ2.

Breast Cancer Genes: BRCA1, BRCA2 and BARD1

Genome stability is a crucial aspect of any living organism. It is essential to cope with DNA damages and to repair them properly. Many human diseases, especially cancer, are linked to different kinds of defects in DNA repair mechanisms which might lead to chromosome abnormalities or uncontrolled proliferation. Defects in DNA repair or recombination genes often predispose humans to cancer development, as it is seen for instance in patients of Bloom and Werner syndrome or breast cancer. Those diseases are linked to mutations in genes whose encoded proteins function as DNA repair proteins. Usually, cancer is not due to a single mutation, but a certain mutation might lead to a higher susceptibility for developing cancer. As breast cancer is the most prevalent cancer worldwide many studies have been made to identify and to understand the role of certain breast cancer factors. In 1994, the first gene which seemed to be genetically linked to the development of hereditary breast cancer was identified [1]. This gene was called B*reast Cancer Susceptibility Gene 1* (BRCA1). Besides BRCA1, another breast cancer gene was identified the following year and named BRCA2 [2]. Later on, it could be shown that both proteins are important factors for homologous recombination (HR) during DNA repair.

As proteins are often part of different complexes and their function depends on certain interactions, there are several known proteins, which are important for the function of BRCA1. The most prominent interaction partner of BRCA1 is the *Breast Cancer Associated Ring Domain Protein* BARD1. The name implies its interaction with BRCA1 via their RING domains. **Figure 1A** shows the general structure of the human breast cancer proteins. Homologs of these genes were identified in several other organisms as well, and interestingly also in the model plant A. thaliana [3-5].

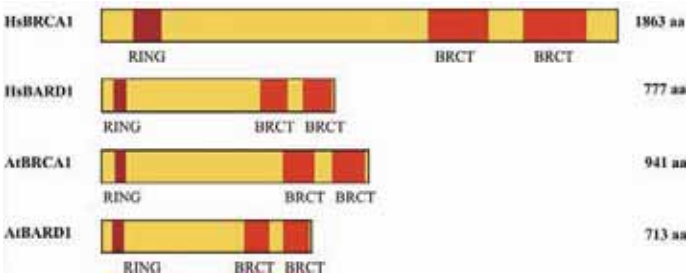

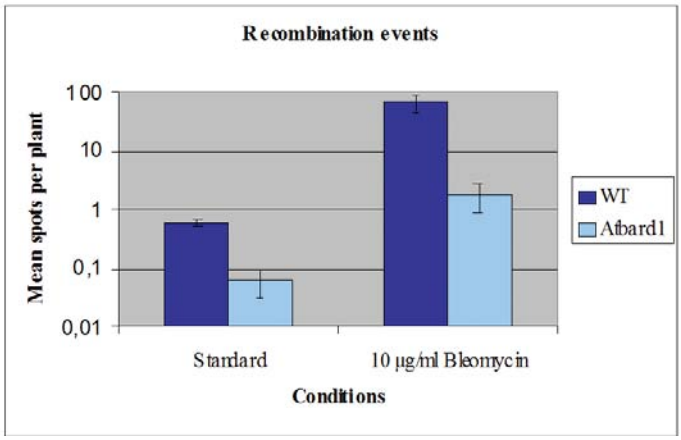

Figure 1 Structure of human and plant breast cancer proteins and the AtBARD1 function during HR. **(A)** The characteristic features of breast cancer proteins are the N-terminal RING and the C-terminal BRCT domains. Both domains are important for protein-protein interactions and the proper functions of the proteins. RING = Really Interesting New Gene; BRCT = BRCA1 C-terminal; Hs = Homo sapiens; At = Arabidopsis thaliana. **(B)** The *Atbard1* mutant plants show a reduction of HR under standard conditions in comparison to the wild type (WT). After induction of double stranded breaks with Bleomycin, the wild type shows a clear induction of HR. The HR in *Atbard1* mutant plants after induction with Bleomycin is less induced, indicating a role for *AtBARD1* in HR. The diagram shows the mean number of blue spots per plant (bars show the SD) from three different experiments with a logarithmic scale for a better presentation.

University of Karlsruhe, Department of Botany II, Karlsruhe, Germany

* Corresponding author. E-mail: holger.puchta@bio.uka.de

Q.Y. Shu (ed.), Induced Plant Mutations in the Genomics Era. Food and Agriculture Organization of the United Nations, Rome, 2009, **118-121**

Structure of plant homologs

As mentioned above, in *A. thaliana* and other plants, gene homologs of BRCA1, BRCA2 and BARD1 were identified. *AtBRCA1* and *AtBARD1* are single copy genes, whereas *AtBRCA2* is a duplictaed gene. The homology between the breast cancer genes and their plant orthologs is mainly conserved in the region of their functional domains. Both BRCA1 and BARD1 possess an N-terminal RING and two C-terminal BRCT-domains. The RING domain of AtBRCA1 has 34% identity and 61% similarity to the human ortholog, whereas the homology of the BRCT region has 28% identity and 61% similarity [4]. The alignment of AtBARD1 with HsBARD1 shows 22% identity and 38% similarity [5]. The RING domain is a protein interaction domain, which is necessary for the E3-Ubiquitin Ligase function of BRCA1 and BARD1 alone as well as for the respective heterodimer. The function of the BRCT domains is based on interactions with phosphopeptides and might therefore be important for regulatory processes. Both BRCA1/BARD1 and BRCA2 play essential roles during mitotic and/or meiotic DNA repair and recombination events. Their essential role in mammals is shown in early embryonic lethality of homozygous BRCA1, BARD1 and BRCA2 mutant mice [6-8]. Interestingly, in *A.thaliana* homozygous single mutant plants of the breast cancer genes are, in contrast to their mammalian counterparts, not lethal. This offers a unique system for studying putative, conserved functions of these breast cancer genes in a higher eukaryotic organism.

Functional Analysis in Plants

BRCA1 and BARD1 are important factors of homologous recombination in somatic cells. Studies in different organisms led to the conclusion that this function seems to be conserved. Via a recombination assay system for *A.thaliana*, it was shown that the At*bard1* single mutants display a defect in homologous recombination and that they are sensitive to MMC, which leads to DNA cross links [5]. **Figure 1B** shows the clear reduction of HR in At*bard1* mutant plants under standard as well as under genotoxic conditions indicating a role for AtBARD1 in HR. AtBRCA2 is also important for HR and plays an essential role during meiosis [3]. As the genome of *A.thaliana* harbors two almost identical homologs, those proteins might have a redundant function.

Research on the function of breast cancer genes in plants might give insight into conserved functions of those genes, as well as reveal plant specific functions. Our present studies concentrate on other proteins that interact with breast cancer proteins. One such family is the RecQ family, whose proteins are also linked to several human diseases.

RecQ helicases as genomic caretakers

Out of the five human homologs of *E. coli* RecQ, mutations in three of them have been shown to result in severe autosomal recessive hereditary diseases. Bloom Syndrome (BS), Werner Syndrome (WS) and Rothmund-Thomson Syndrome (RTS) result from biallelic loss-of-function mutations in the genes BLM, WRN or HsRECQ4, respectively. Patients diagnosed with the disorders RAPADILINO Syndrome and Baller-Gerold Syndrome (BGS) have recently been shown to carry mutations in the HsRECQ4 gene as well.

All of these syndromes result in a set of common characteristics, for example genomic instability and a predisposition to cancer malignancies [9]. However, there are also syndrome-specific features and unique cellular and genetic defects that suggest non-redundant cellular functions for these RecQ helicases. BS patients present with a proportional growth deficiency, skin abnormalities, such as sun sensitivity, hypo- and hyperpigmentation, fertility defects and changes in fat and sugar metabolism [10]. Notably, there is an increased predisposition to all types of cancer with high incidence. In BS fibroblasts, the hallmark characteristic is the elevated rate of sister chromatid exchanges due to increased homologous recombination.

Shortly after the connection of BLM with BS, it was shown that mutations in the WRN gene are causative for the recessive disorder Werner Syndrome [11,12]. WS is a progeroid disease resulting in premature aging that develops during the second decade of life and is associated with age-related disorders like greying and loss of hair, skin atrophy, atherosclerosis, osteoporosis, bilateral cataracts and type II diabetes mellitus. WS is also associated with a high incidence of cancer, but contrary to BS patients, individuals with WS show a predisposition primarily to sarcomas. On the cellular level, WS manifests in genomic instability due to chromosome breaks, reciprocal chromosomal translocations and genomic deletions.

The third and only other human RecQ helicase that has been associated with a disease is HsRECQ4, mutated in about 60% of all persons diagnosed with Rothmund-Thomson Syndrome [13]. RTS manifests in skeletal abnormalities, poikiloderma (skin atrophy and dyspigmentation), cataracts, hypogonadism, early greying and loss of hair. The cancer predisposition typical for RecQ-related disorders is seen in RTS as well, but it is restricted mainly to osteosarcomas.

RecQ helicases in plants

In total, there are seven different RecQ like genes present in the model plant *A.thaliana* (**Fig. 2**). As mentioned before, mutations in the human gene coding for the BLM protein lead to a severe genetic disorder called Bloom syndrome [12]. On the sequence level, two of them, At*RECQ4A* and At*RECQ4B*, can be considered putative Hs*BLM* homologs. Regarding the conserved domains within the seven helicase motifs, both proteins share a sequence identity of approximately 53% with the HsBLM protein, and incidentally about 46% with the yeast RecQ homolog SGS1.

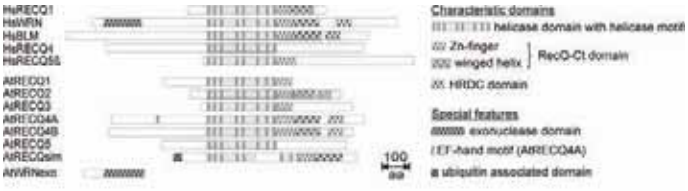

Figure 2 Human and Arabidopsis RecQ homologs. The typical structure of RecQ helicases is found in virtually all members of this family. The RecQ helicase domain, the RecQ-Ct- and the HRDC domain (Helicase and RNAse D C-terminal) are most common, whereas the exonuclease domain is only found in the WRN protein, and the EF-hand motif only in AtRECQ4A. In plants and insects, the exonuclease domain of the HsWRN protein is coded by a small gene, which seems to be fused in HsWRN.

At*RECQ4A* and At*RECQ4B* exhibit an identity of about 70% regarding their DNA and protein sequences, and have therefore arisen from a recent duplication event [14]. Amazingly, in contrast to their high sequence similarity, mutations in At*RECQ4A* and *4B* lead to oppositional phenotypes respectively. Whereas At*recq4A* reflects the "RecQ typical" phenotype showing sensitivity towards genotoxic agents, such as MMS or cisplatin, At*recq4B* plants are not more affected than the wild type control plants [15,16]. Furthermore, we could show hyperrecombination for At*recq4A*, as it has been shown for other RecQ mutants, such as human *blm* or yeast *sgs1* [15-18]. In contrast to the expected results obtained for At*recq4A* as typical RecQ mutant, in At*recq4B* plants somatic HR is strongly reduced compared to the wild type [15]. This hyporecombination phenotype has not been described for any eukaryotic RecQ mutant so far, and points to a positive involvement of the AtRECQ4B protein in the recombination process.

Another property that seems to be conserved in AtRECQ4A is the interaction with a type 1A topoisomerase. This interaction has directly been shown for yeast SGS1 with TOP3, as well as for the human BLM

protein with HsTOP3α [19]. Due to the severity of the phenotypes, it is problematic to study eukaryotic TOP3α functions with the help of the respective mutants. Nevertheless, we could show very recently for At*recq4A* that this mutation is able to rescue the lethal phenotype of *top3α* mutants in Arabidopsis, resulting in sterile but viable plants [15].

Finally, double mutants of At*mus81* and At*recq4A* develop poorly and die within about two weeks. This is in line with the lethality found in double mutants of the structure-specific endonuclease MUS81 and the respective RecQ homologs of budding and fission yeast, SGS1 and RQH1, which are synthetically lethal. This result points to a high level of conservation of the somatic RECQ and MUS81 functions, such as the involvement of both proteins in two parallel pathways working on stalled replication forks [16].

In both cases, the results obtained for the RecQ double mutants with *mus81* or *top3α*, respectively, are restricted to the *recq4A* mutation of *A. thaliana*, whereas for At*recq4B* no effect on the At*top3α* and At*mus81* phenotypes could be observed [15,16]. Therefore it can be concluded that in *Arabidopsis* RECQ4A, and not RECQ4B, is in most aspects the functional homolog of BLM and SGS1. Nevertheless, the recombination promoting function of RECQ4B might also have originated from a common BLM-like ancestor protein.

Biochemical characterization of AtRECQ2

Whereas the T-DNA insertion mutants enable us to analyze the effect of missing or truncated proteins, biochemical analysis reveals what reactions the proteins are possibly able to catalyze. The two approaches are complementary, with the biochemical analysis a reaction is being tested for feasibility, for example, if a participation in a specific pathway is proposed. However, biochemical analysis does not state whether a specific reaction is really taking place *in vivo*, since it may be influenced, for instance, by post-translational modifications of the protein or by protein interaction partners. On the other hand, with the help of specific information on the types of substrates the enzyme might process, a more focused *in vivo* analysis can be performed.

The method used is briefly introduced here: DNA sequences are designed with complementary and non-complementary stretches in such a way that a specific DNA-structure will form. The DNA structure is built by heating one labeled oligonucleotide (^{32}P) together with the other constituents and cooling them down slowly with subsequent purification. It is incubated with the enzyme under defined conditions. Then, the reaction products are analyzed via native polyacrylamide gel electrophoresis (PAGE), in which the original structure is separated from the product(s). The structures containing a ^{32}P label can be analyzed and quantified allowing the calculation of the percentage of unwinding.

Here, some data of our biochemical characterization of *A. thaliana* RECQ2 is presented [20]. AtRECQ2, together with AtRECQ4A and AtRECQ4B, possess the complete set of (uninterrupted) domains, characteristic for RecQ-helicases, as do HsWRN and HsBLM (Fig. 2). Additionally, AtRECQ2 interacts with AtWRNexo [21]. AtWRNexo is homologous to the exonuclease domain of HsWRN (**Fig. 2**) and biochemical analysis of AtWRNexo has revealed conserved properties [22]. We analyzed the biochemical functions of AtRECQ2 in order to classify it either as orthologous to the HsWRN-helicase or as a potentially plant-specific protein with its own set of functions.

We expressed AtRECQ2 in *E. coli* and successfully purified it with the help of an N-terminal calmodulin binding peptide tag and a C-terminal hexahistidine tag. In order to be able to judge the purity of our AtRECQ2 preparation, we also cloned, expressed and purified AtRECQ2-K117M in an identical fashion. For AtRECQ2-K117M, the substitution of lysine by methionine in the Walker A motif leads to an abolishment of ATPase and therefore helicase activity. Thus, an activity observed in assays with AtRECQ2 that is missing with AtRECQ2-K117M is due to our enzyme of interest.

We were able to show that AtRECQ2 is a (d)NTP dependent 3' to 5' DNA helicase (**Fig. 3A and B**). This can not be taken for granted as for example, no helicase activity was shown for HsRECQ4 [23]. The ability of AtRECQ2 to use all nucleotide cofactors to catalyze unwinding is not common for RecQ helicases. These properties are only similar to those of HsWRN helicase, for which ATP and dATP are best as well, followed by dCTP and CTP. Strand unwinding by HsWRN can also be measured with GTP, dGTP, UTP and dTTP but it is not efficient [24]. All other RecQ-homologs analyzed for the usage of different (d)NTPs are more restricted.

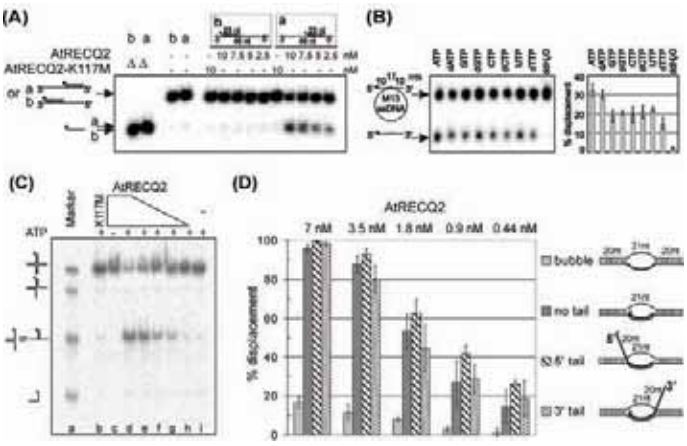

Figure 3 Biochemical analysis of AtRECQ2 [20]. **(A)** AtRECQ2 is a 3'-5'DNA helicase. The substrates are schematically drawn in the dotted boxes; * marks the ^{32}P-label. The arrows indicate the positions of migration of the substrates (top) or the 23 nt – unwinding products of substrate a (unwound by 3' 5' helicases) and b (unwound by 5' 3' helicases), respectively (bottom). The reactions with AtRECQ2-K117M show no unwinding, thus the AtRECQ2 preparation is devoid of helicase contamination. μ heat-denatured substrate. **(B)** AtRECQ2 can use different nucleotide-triphosphates for unwinding. Helicase data are presented as autoradiogram and as mean with SD. For the respective reactions ATP was substituted by dATP, GTP, dGTP, CTP, dCTP, UTP, dTTP and water. **(C)** AtRECQ2 can branch migrate Holliday Junctions. Autoradiography of the reaction products. In reaction c ATP was omitted. It is clearly visible that the main product of AtRECQ2 is splayed arm, indicative for branch migration. **(D)** Quantification of helicase data (mean and SD) of reactions with a bubble and different D-Loop-structures, schematically drawn on the right. The invading strands of the D-Loop structures were unwound. No significant preference for a special D-Loop structure can be observed with different AtRECQ2 concentrations used.

The reaction of AtRECQ2 was also analyzed on DNA substrates that mimic recombination intermediates: a partially mobile Holliday Junction and different D-Loops (**Fig. 3C and 3D**). The analysis of the reaction of AtRECQ2 on Holliday Junctions reveals splayed arm products, characteristic for branch migration. As it was shown before by others, splayed arm is the main product of many RecQ-helicases - also for HsWRN [25]. D-Loops are formed in an early step of homologous recombination, when an ssDNA invades the homologous dsDNA and pairs with the complementary strand of the duplex. AtRECQ2 can displace invading strands of D-Loops, regardless if there is a protruding ssDNA or not, and irrespectively of the protruding ssDNA's directionality. The analyzed bubble was partly unwound. Melting of productive D-Loops in which the 3' end of ssDNA is invading can be considered as anti-recombinogenic. Also, unwinding of the unproductive D-Loops with 5' invasions and 3' protruding tails by RecQ-helicases may be important. The data of other RecQ helicases on their action on D-Loops are published. Whereas some RecQ proteins show a preference for 3' tailed D-Loops, the properties of HsWRN [26] are similar to those of AtRECQ2: the invading strands of all three D-Loop substrates are similarly well displaced.

To sum up, the biochemical properties of AtRECQ2 are closest to those of HsWRN. Therefore, the hypothesis that those two are functionally homologous is reinforced and it will be highly interesting to see

whether the future analysis of the respective T-DNA insertion mutants will sustain this conclusion.

In general, we can summarize that a reasonable number of genes involved in genome stability and cancer predisposition in animals are well-conserved in plants. The function of these genes is often similar on a general level, such as the preservation of genome stability, as well as regarding their biochemical properties. Nevertheless, besides helping to understand basic mechanisms of genome stability in eukaryotes, our research also has a strong biotechnological potential. A better understanding of homologous recombination in plants might help us to set up new approaches in green gene technology, such as gene targeting or improved breeding.

ACKNOWLEDGEMENTS

We want to thank S. Blanck, K. Demand, W. Reidt, R. Wurz-Wildersinn, S. Hettinger, C. Moock, S. Buss and S. Zeiler for their contribution to this article. We want to apologize that, due to space limitation, we were not able to cite all the relevant literature. This work was supported by DFG grants HA5055/1-1 and PU137/10-1.

BIBLIOGRAPHY

1. Miki, Y. *et al.* A strong candidate for the breast and ovarian cancer susceptibility gene BRCA1. *Science* **266,** 66–71 (1994).
2. Wooster, R. *et al.* Identification of the breast cancer susceptibility gene BRCA2. *Nature* **378**, 789-92 (1995).
3. Siaud, N. *et al. Brca2* is involved in meiosis in *Arabidopsis thaliana* as suggested by its interaction with *Dmc1*. *Embo J.* **23**, 1392–1401 (2004).
4. Lafarge, S., And Montane, M.H. Characterization of *Arabidopsis thaliana* ortholog of the human breast cancer susceptibility gene 1: *AtBRCA1*, strongly induced by gamma rays. *Nucleic Acids Res* **31**, 1148-55 (2003).
5. Reidt, W., Wurz, R., Wanieck, K., Chu, H.H., Puchta, H. A homologue of the breast cancer-associated gene BARD1 is involved in DNA repair in plants. *Embo J.* **25**, 4326-37 (2006).
6. Sharan, S.K. *et al.* Embryonic lethality and radiation hypersensitivity mediated by Rad51 in mice lacking Brca2. *Nature* **386**, 804-810 (1997).
7. Gowen, L.C. *et al. Brca1* deficiency results in early embryonic lethality characterized by neuroepithelial abnormalities. *Nature Genetics* **12**, 191-94 (1996).
8. Mccarthy, E.E., Celebi, J.T., Baer, R., Ludwig, T. Loss of Bard1, the heterodimeric partner of the Brca1 tumor suppressor, results in early embryonic lethality and chromosomal instability. *Mol Cell Biol* **23,** 5056–63 (2003).
9. Ouyang, K.J., Woo, L.L., Ellis, N.A. Homologous recombination and maintenance of genome integrity: Cancer and aging through the prism of human *RecQ* helicases. *Mech Ageing Dev.* Mar 15 [Epub Ahead Of Print] (2008).
10. German, J., Sanz, M.M., Ciocci, S., Ye, T.Z., Ellis, N.A. Syndrome-causing mutations of the BLM gene in persons in the Bloom's Syndrome Registry. *Hum. Mutat.* **28,** 743-53 (2007).
11. Yu, C.E. *et al.* Positional cloning of the Werner's syndrome gene. *Science* **272**, 258-62 (1996).
12. Ellis, N.A. *et al.* The Bloom's syndrome gene product is homologous to *RecQ* helicases. *Cell* **83**, 655-66 (1995).
13. Kitao, S. *et al.* Mutations in RECQL4 cause a subset of cases of Rothmund-Thomson syndrome. *Nat Genet.* **22**, 82-84 (1999).
14. Hartung, F., Puchta, H. The RecQ gene family in plants. *Journal Of Plant Physiology* **163**, 287-296 (2006).
15. Hartung, F., Suer, S., Puchta, H. Two closely related RecQ-helicases have antagonistic roles in homologous recombination and DNA repair in *Arabidopsis thaliana*. *Proc Natl Acad Sci Usa* **104**, 18836-841 (2007).
16. Hartung, F., Suer, S., Puchta, H. The Role of AtMUS81 in DNA Repair and its Genetic Interaction with the Helicase *AtRecQ4A*. *Nucleic Acids Res.* **34**, 4438-48 (2006).
17. Watt, P.M., Louis, E.J., Borts, R.H., Hickson, I.D. Sgs1: a eukaryotic homolog of E. coli RecQ that interacts with topoisomerase II *in vivo* and is required for faithful chromosome segregation. *Cell* **81**, 253-60 (1995).
18. Langlois, R.G., Bigbee, W.L., Jensen, R.H., German, J. Evidence for increased in vivo mutation and somatic recombination in Bloom's syndrome. *Proc Natl Acad Sci Usa* **86**, 670-4 (1989).
19. Mankouri, H.W. And Hickson, I.D. The RecQ helicase-topoisomerase III-Rmi1 complex: a DNA structure-specific 'dissolvasome'? *Trends Biochem Sci.* **32**, 538-46 (2007).
20. Kobbe, D., Blanck, S., Demand, K., Focke, M., Puchta, H. AtRECQ2, a RecQ-helicase homologue from *Arabidopsis thaliana*, is able to disrupt different recombinogenic DNA-structures *in vitro*. *Plant J.* **55**, 397-405 (2008).
21. Hartung, F., Plchova, H., Puchta, H. Molecular characterisation of RecQ homologues in *Arabidopsis thaliana*. *Nucleic Acids Res.* **28**, 4275-82 (2000).
22. Plchova, H., Hartung, F., Puchta, H. Biochemical characterization of an exonuclease from Arabidopsis thaliana reveals similarities to the DNA exonuclease of the human Werner syndrome protein. *J. Biol. Chem.* **45**, 44128-138 (2003).
23. Macris, M.A., Krejci, L., Bussen, W., Shimamoto, A., Sung, P. Biochemical characterization of the RECQ4 protein, mutated in Rothmund-Thomson syndrome. *DNA Repair (Amst).* **5**, 172-80 (2006).
24. Shen, J.C., Gray, M.D., Oshima, J., Loeb, L.A. Characterization of Werner syndrome protein DNA helicase activity: directionality, substrate dependence and stimulation by replication protein A. *Nucleic Acids Res.* **26**, 2879-85 (1998).
25. Mohaghegh, P. *et al.* The Bloom`s and Werner`s syndrome proteins are DNA structure-specific helicases. *Nucleic Acids Res.* **34**, 2269-79 (2001).
26. Orren, D.K., Theodore, S., Machwe, A. The Werner syndrome helicase/exonuclease (WRN) disrupts and degrades D-loops *in vitro*. *Biochemistry* **41**, 13483-8 (2002).

Genomic and Gene-specific Induction and Repair of DNA Damage in Barley

V Manova*, M Georgieva, B Borisov, B Stoilova, K Gecheff & L Stoilov

Abstract

Repair of DNA damage induced by various mutagenic agents within the barley genomic and ribosomal DNA was the subject of investigation. Reconstructed karyotypes T-1586 and T-35, with normal and increased expression of ribosomal genes respectively, were utilized to evaluate the relationship between the transcriptional activity and the rate of DNA damage induction and their repair. A tendency towards restoration of rDNA integrity after γ-irradiation was observed, indicative for the efficient recovery of double-strand breaks in barley ribosomal DNA. Ability of barley ribosomal genes to cope with damage produced *in vivo* by the radiomimetic agent bleomycin was further analyzed. Preferential sensitivity of barley linker DNA towards bleomycin treatment *in vivo* was established. Fragments containing intergenic spacers of barley rRNA genes displayed higher sensitivity to bleomycin than the coding sequences. No heterogeneity in the repair of DSB between transcribed and non-transcribed regions of ribosomal genes was detected. Data indicated that DSB repair in barley ribosomal genes, although relatively more efficient than in genomic DNA, did not corelate with NOR activity. Repair kinetics of UV-C induced cyclobutane pyrimidine dimers in barley genomic and ribosomal DNA was also studied. Less cyclobutane pyrimidine dimers (CPD) in rDNA in comparison to total genomic DNA was detected. Results showed that UV-C induced CPD in barley ribosomal genes are as efficiently repaired as in the rest of the genome predominantly by light repair mechanisms.

Introduction

Maintenance of DNA integrity by the cellular repair mechanisms is an essential function of living organisms, preserving the genuine status of their genetic information. DNA repair mechanisms are also not fully correct, which increases the genetic diversity and variability of the populations. The biological consequences of non-repaired or miss-repaired DNA damage depend on the type and frequency of the lesions as well as on the functional characteristics and location of the target DNA. Therefore, the investigations on the selective induction and differential efficiency of repair processes in individual genes and defined DNA sequences are of substantial theoretical and practical importance.

Many studies have shown that the heterogeneity of DNA damage induction and repair, dependent on chromatin organization, transcriptional activity and nature of individual DNA sequences, is a widely spread phenomenon in higher eukaryotes. A crucial breakthrough in the topic of differential repair was the finding that actively transcribed genes are more quickly repaired by nucleotide excision repair (NER) than non-expressed ones. It was further demonstrated that such preferential recovery of active genes was mainly due to the accelerated repair of lesions in the transcribed DNA strand [1, 2]. Moreover, intragenic repair heterogeneity, reflecting chromatin alterations along the genes was also established [3, 4]. After the initial observation for strand-specific repair of cyclobutane pyrimidine dimers, the link between DNA repair and transcription for other types of DNA lesions has been extensively studied. Recovery from damage induced by UV, crosslinking and alkylating agents in mammalian ribosomal (rRNA) genes, however, was found to be less effective than in genes transcribed by RNA polymerase II or in the genome overall [5-7]. Efficient, but not preferential, repair was observed for bleomycin and IR-induced strand breaks in mammalian rRNA genes [8, 9] indicating that repair of rDNA might be rather lesion-dependent than tightly linked to transcription. Recently, however, a transcription-dependent repair of UV-induced CPD in yeast rRNA genes accomplished by NER and photoreactivation has been demonstrated [10]. Studies on the gene-specific induction and repair of DNA damage in plants, however, are limited and there is a lack of information about the existence of preferential DNA repair of active plant genes in relation to their transcriptional activity, chromatin structure and genomic location.

Description of the activities performed

Our main research activities were focused on the genomic and gene-specific induction and repair of DNA damage in barley. The induction and repair kinetics of double-strand breaks (DSB) in barley ribosomal DNA (rDNA) after treatment of root tips with ionizing radiation and bleomycin were investigated. The relationship between transcriptional activity of ribosomal genes and the efficiency of induction and repair of these lesions in whole barley repeats, as well as in the transcribed and non-coding rDNA sequences were also analyzed. Formation and repair of CPD in genomic (gDNA) and ribosomal DNA after UV-C irradiation of barley leaves were also a subject of investigation.

Ionizing radiation-reconstructed barley karyotypes T-1586 and T-35 characterized with normal and increased activity of Nucleolus Organizing Regions (NOR) were utilized to study the link between the repair potential of barley ribosomal genes and their expression. Line T-35 is derived from T-1586 and contains deletion of the NOR-bearing segment of chromosome 6H. As a result, a higher activity of the remaining rRNA gene cluster localized in NOR 5H was observed [11, 12]. Barley ribosomal genes are represented by long (9.8 kb) and short (8.8 kb) ribosomal repeats, localized in the NOR of chromosome 6H and 5H respectively (**Fig. 1**).

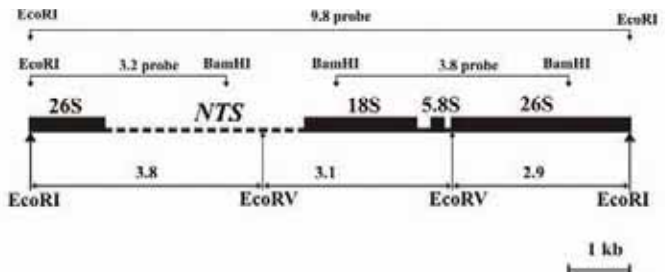

Figure 1 Partial restriction map of the longer 9.8kb barley rDNA repeat (clone HV 014). Solid and dotted lines represent coding regions and non-transcribed intergenic spacer respectively.

Institute of Genetics "Acad. D. Kostoff", Bulgarian Academy of Sciences

* Corresponding author. E-mail: vmanova@bas.bg

Repair of ionizing-radiation induced DSB in barley ribosomal genes

Ionizing radiation was initially used for generation of DSB in barley ribosomal DNA. Kinetics of DSB induction obtained after treatment of germinating seeds from karyotypes T-1586 and T-35 with gamma-rays is outlined in **Fig. 2**. It was found that 100Gy gamma-rays produce DSB in rDNA, resulting in a detectable decrease of the corresponding hybridization signal. Although the yield of DSB in both rDNA repeats immediately after irradiation was relatively low, after a further three hours of germination a higher amount of DNA damage in the respective gene clusters was detected. After a 24-hour recovery of the root seedlings, the integrity of rDNA reached the control values. These data indicate the existence of efficient recovery mechanisms for DSB in barley rDNA. The observed lack of correlation between the expression of barley rRNA genes and their sensitivity against radiation-induced damage is in accordance with the proposed uniform distribution of the repair activities responsible for double-strand breaks in mammalian cells. The results favour a mechanism for induction of DSB in barley ribosomal genes, presumably uncoupled with their transcription [13].

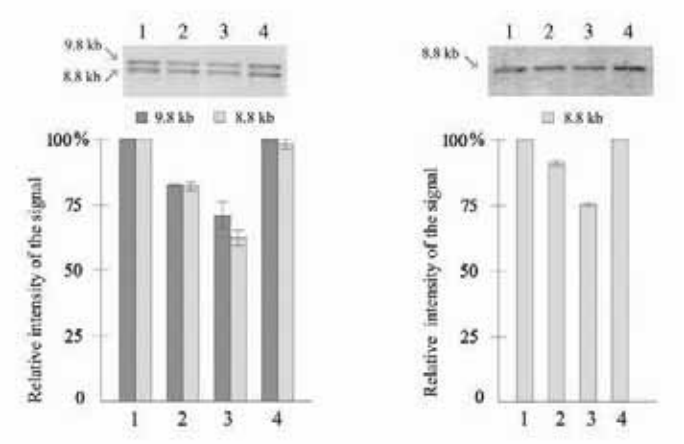

Figure 2 Hybridization profiles of rDNA repeats and histogram representation of the densitometric data (in arbitrary units) obtained after irradiation of germinating seeds from karyotype T-1586 and deletion line T-35. Intensity of the signal in the untreated control sample is taken as 100%. Lane 1, 2, 3 and 4 - control, 0, 3 and 24 hours recovery.

Repair of bleomycin-induced double-strand breaks in barley genomic DNA and ribosomal genes

Repair kinetics of damage induced by bleomycin (200μg/ml) in barley genomic DNA was assessed by conventional gel electrophoresis under neutral and alkaline conditions for DSB and SSB respectively (**Fig. 3**). A distinctive feature of DSB profiles was their nucleosomal-phased fragmentation due to the higher sensitivity of barley linker DNA towards bleomycin treatment *in vivo*.

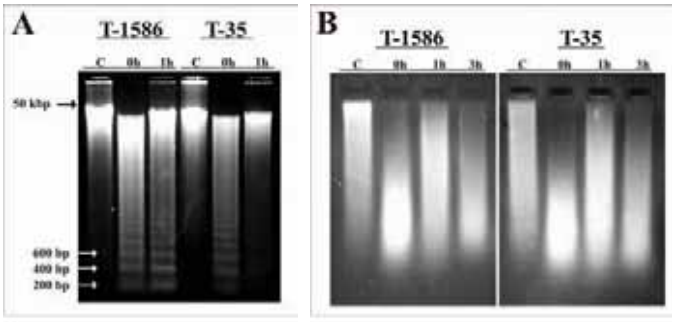

Figure 3 Neutral **(A)** and alkaline **(B)** ethidium bromide-stained gels visualizing the induction and repair of DSB **(A)** and SSB **(B)** in barley genomic DNA. C - untreated DNA; 0h, 1h and 3h – recovery periods after bleomycin treatment.

Comparison of the yields of initially induced DSB in ribosomal and genomic DNA revealed an increased sensitivity of gDNA, whereas rDNA was somewhat more resistant to DSB induction by bleomycin. Taking into account that in barley only a small proportion of about 4000 rRNA genes is actively transcribed, chromatin compactness appeared as one of the possible factors determining the observed differences. Data showed efficient repair of bleomycin-induced SSB and DSB in genomic DNA of both karyotypes after one hour of repair. Recovery kinetics of DSB in ribosomal DNA generally followed that found in genomic DNA (**Fig. 4**). Both lines displayed even higher capacity for repair of DSB in rDNA compared to bulk DNA. At first glance, repair of ribosomal genes in T-35 appears to be more effective than in T-1586, but this could actually reflect the overall repair capacity of this line. On the other hand, the existence of putative inactive rDNA repeats still residing in NOR 5H might obscure the visualization of fast repair in transctribed genes. As a whole, however, the results support the notion that the repair efficiency of bleomycin-induced DSB in barley ribosomal genes was not substantially affected by the overall activity of the respective barley NORs [14].

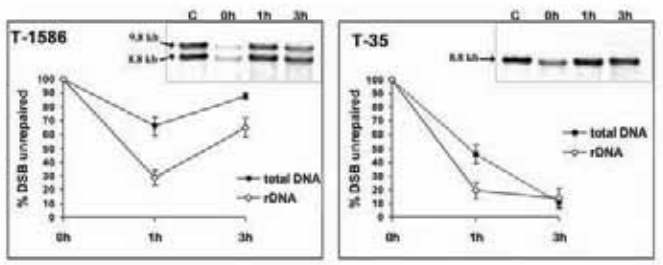

Figure 4 Comparative data representing the efficiency of DSB repair in rDNA and total genomic DNA from karyotypes T-1586 and T-35. Initial rate of DSB, measured at time point 0h was assumed as 100% damage. Accordingly, repair levels were expressed as percentage of DSB left unrepaired during the recovery periods (one hour and three hours).

Comet assay was applied to analyze the induction and repair kinetics of DSB and SSB produced by bleomycin in barley supercoiled DNA loop domains (**Fig. 5**). Data have shown an effective repair of DSB within the first 15 minutes after application of bleomycin to barley root tips. Percentage of the remaining damage after one hour of repair was about 50% from the initial one after treatment with a lower bleomycin dose. Surprisingly, an even more pronounced recovery was observed after application of the highest bleomycin concentration (**Fig. 6**).

Figure 5 Microphotographs of the representative comet images obtained after application of neutral (A) and alkaline (B) comet assay.

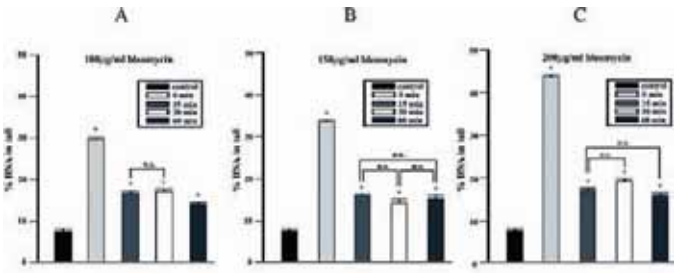

Figure 6 DSB repair based on% DNA in tail (±SE) in Hordeum vulgare root tips cells at various recovery periods after treatment with bleomycin. **(A)**:100 μg/ml; **(B)**: 150 μg/ml; **(C)**: 200 μg/ml. *GLM (P<0.001). n.s. No significant differences.

The frequency of initially induced SSB was not substantially influenced by the bleomycin concentrations applied. Observed repair efficiency was significantly higher at 50μg/ml shortly after treatment and remained steady afterward. After application of 100μg/ml, however, at least one hour of recovery was necessary for the cells to reach the levels of DNA damage detected 15 minutes after treatment with the lower bleomycin concentration (**Fig. 7**) [15].

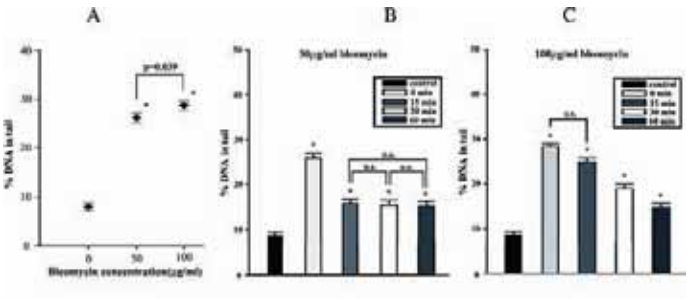

Figure 7 Initial induction **(A)** and recovery kinetics **(B, C)** of DNA breaks induced by bleomycin detected by alkaline comet assay. *GLM (P<0.001). n.s. No significant differences.

Induction and repair of DSB in defined domains of barley ribosomal genes

As the ribosomal repeat comprises sequences with different chromatin organization and transcriptional status, the induction and repair of bleomycin-induced DSB within the defined regions of ribosomal genes was analyzed. Data for the number of initially induced DNA damage showed preferential induction of DSB within the fragments comprising non-transcribed sequences (3.8 kb and 2.8 kb respectively), in comparison to that covering the structural part of the genes (fragments 3.1 kb and 2.9 kb) (**Fig. 8**).

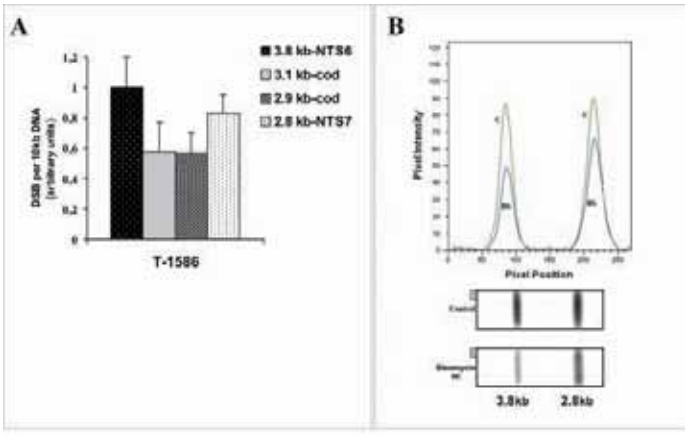

Figure 8 (A) Differential distribution of DSB within specific regions of barley ribosomal genes. Double-digested DNA from line T-1586 was hybridized consecutively with 3.2kb probe (detecting the non-transcribed spacers) and 3.8kb probe (for the coding regions only). **(B)** Densitometric and hybridization profiles of 3.8kb and 2.8kb non-transcribed spacers from both rDNA clusters in line T-1586, obtained with the 3.2kb probe: 1- control, 2- immediately after bleomycin treatment.

On the other hand, we did not found substantial differences between the repair kinetics of bleomycin-induced DSB within the transcribed and non-transcribed ribosomal sequences (**Fig. 9**). To our knowledge, data on the induction and repair of damage in specific regions of plant genes have not been previously reported. Increased sensitivity to DSB found in barley non-transcribed spacer might reflect a higher density of repeated elements with enhancer and promoter functions, which in concert with the relatively relaxed chromatin structure, might render this area more vulnerable to damage induction. Lack of differential repair efficiency in transcribed and non-transcribed regions of barley ribosomal genes in both lines, implied that their distinct transcription-dependent chromatin organization did not influence the repair of bleomycin-induced DSB in these specific domains. Our data indicated that the repair of this damage in barley rRNA gene clusters, although more efficient than in total genomic DNA, did not correlate with the overall NOR activity [14].

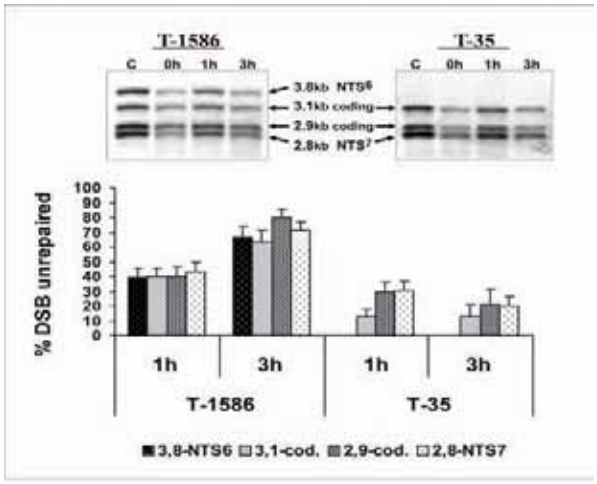

Figure 9 DSB repair efficiency within specific regions of barley ribosomal genes of karyotypes T-1586 and T-35. Repair was expressed as percentage of DSB left in the ribosomal fragments during the recovery periods (one and three hours). Representative Southern blots obtained after hybridization with 9.8kb probe of EcoRI/EcoRV-digested control and treated DNA, in order to differentiate the coding from spacer regions of rDNA repeats, are also inserted.

Induction and repair of CPD in barley genomic and ribosomal DNA

Barley seedlings were irradiated with various UV-C doses in the range 0.5-5 J/cm^2 and subsequently incubated for different repair intervals. CPD repair was investigated at the level of genomic and ribosomal DNA in the first leaf of six-day-old seedlings under light and dark conditions. Data showed obvious prevalence of light repair mechanisms in barley leaves even after high doses of UV-C irradiation. Less amount of CPD in rDNA in comparison to total genomic DNA immediately after irradiation was detected. Kinetics of CPD repair was found to be similar in the genomic and ribosomal DNA (unpublished data). These results indicate that UV-C induced CPD in barley ribosomal genes are as efficiently repaired as in the rest of the genome (**Fig. 10**).

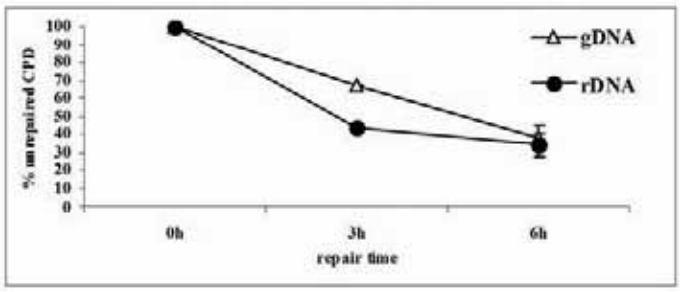

Figure 10 Efficiency of light CPD repair in barley genomic and ribosomal DNA.

Conclusions

Altogether, the data suggested the operation of efficient repair mechanisms maintaining the integrity of barley total genomic DNA and

ribosomal genes after treatment with different types of mutagenic agents such as ionizing radiation, bleomycin and UV-C light. The results also showed that, particularly for IR and bleomycin induced DSB, there was no noticeable relationship between the transcriptional activity of rRNA genes and their repair potential.

ACKNOWLEDGEMENTS
This work was supported by the IAEA Research contract № Bul 12608/RO/RBF and grants from Bulgarian National Science Fund - Genomics Programme, Contract No G-1-01 and Grant No K-804.

BIBLIOGRAPHY

1. Mellon, I., Spivak, G., Hanawalt, P.C. Selective removal of transcription blocking DNA damage from the transcribed strand of the mammalian DHFR gene. *Cell* **51**, 241-249 (1987).

2. Friedberg, E.C. Relationship between DNA repair and transcription. *Annu. Rev. Biochemistry* **65**, 15-42 (1996).

3. Hu, W., Feng, Z., Chasin, L.A., Tang, M.-S. Transcription-coupled and transcription-independent repair of cyclobutane pyrimidine dimers in the dihydrofolate reductase gene. *J. Biol. Chem.* **277**, 38305-38310 (2002).

4. Meier, A., Thoma, F. RNA polymerase I transcription factors in active yeast rRNA gene promoters enhance UV damage formation and inhibit repair. *Mol. Cell. Biol.* **25**, 1586 - 1595 (2005).

5. Stevnsner, T., May, A., Petersen, L.N., Larminat, F., Pirsel, M., Bohr, V.A. Repair of ribosomal RNA genes in hamster cells after UV irradiation, or treatment with cisplatin or alkylating agents. *Carcinogenesis* **14**, 1591-1596 (1993).

6. Christians F.C., Hanawalt, P.C. Lack of transcription-coupled repair in mammalian ribosomal RNA genes, *Biochemistry* **32**, 10512-10518 (1993).

7. Fritz L.K., Smerdon, M.J. Repair of UV damage in actively transcribed ribosomal genes, *Biochemistry* **34**, 13117-13124 (1995).

8. Fritz, L.K., Suquet, C., Smerdon, M.J. Strand breaks are repaired efficiently in human ribosomal genes. *J.Biol. Chem.* **271**, 12972-12976 (1996).

9. Ljungman, M. Repair of radiation-induced DNA strand breaks does not occur preferentially in transcriptionally active DNA. *Radiat. Res.* **152**, 444-449 (1999).

10. Meier, A., Livingstone-Zatchej, M., Thoma, F. Repair of active and silenced rDNA in yeast: the contributions of photolyase and transcription-coupled nucleotide excision repair. *J. Biol. Chem.* **277**, 11845-11852 (2002).

11. Gecheff, K. Cytogenetic study on a barley translocation line and some conclusions concerning chromosome karyogram designation. *Genet. Pl. Breed.* **11**, 17-22 (1978).

12. Gecheff, K.I., Chvarleva, T., Georgiev, S., Wilkes, T., Karp, A. Cytological and molecular evidence of deletion of ribosomal RNA genes in chromosome 6 of barley (*Hordeum vulgare* L). *Genome* **37**, 419-425 (1994).

13. Manova, V.I., Stoilov, L. Induction and recovery of double-strand breaks in barley ribosomal DNA, *DNA Repair (Amst.)* **2**, 983-990 (2003).

14. Manova, V., Gecheff, K., Stoilov, L. Efficient repair of bleomycin-induced double-strand breaks in barley ribosomal genes. *Mutat. Res.* **601**, 179–190 (2006).

15. Georgieva, M., Stoilov, L. Assessment of DNA double-strand breaks produced by bleomycin in barley genome by the comet assay. Env. *Mol. Mutagen.* **49**, 381-387 (2008).

An Approach to Screen and Identify Novel Meiotic Mutants in an EMS Mutant Population

J A da Costa-Nunes* & W Viegas

Abstract

A novel *Arabidopsis* EMS mutant population was produced aiming at identifying until now unknown meiotic mutants. The M_2 EMS mutant families were first screened for their reduced fertility. These plants with a reduced fertility were subjected to a second screening at the cytological level. Plants with abnormal meiosis, namely abnormal chromosome segregation and chromosome fragmentation were selected for further characterization and SNP mutation mapping. So far, 232 sterile and semi-sterile M_2 candidates have been identified in the fertility screen, of which 110 sterile mutants were further analyzed at the cellular level; 15 of these have been analysed at the cytological level. Mapping has been carried out.

Abbreviations

EMS - ethylmethanesulfonate; SNP - Single Nucleotide Polymorphism; M_1 - plants obtained from seeds exposed to EMS; M_2 and M_3 - plants obtained from seeds produced by self-fertilization of M_1 and M_2 plants, respectively; F1 - plants obtained from cross of two different landraces; F_2 - plants obtained from self-fertilization of F_1 plants.

Introduction

During meiosis two major events occur, DNA recombination and two sequential chromosomal segregations. Meiotic DNA recombination takes place between homologous chromosomes and it requires the formation of DNA double strand breaks, strand exchange for repair, and resection and resolution of the entangled recombined DNA strands originated from the two-paired homologous chromosomes. These homologous chromosomes segregate after recombination has occurred, and only during the second division do the sister chromatids segregate [1]. Consequently, in *Arabidopsis* male meiocytes, during the fist meiotic division the 10 chromosomes are segregated to the two opposite ends of the cell as five-chromosome units; during the second meiotic division the two groups of homologues divide again, segregating five sister chromatids to each end [2]. The final products of the male meiotic division are four evenly sized haploid cells that remain attached until just after meiosis as a tetrad; the tetrad eventually breaks down and the haploid cells become individualized microspores. In *qrt1/qrt1* mutants however, the four haploid products of meiosis remain in a tetrad even during microsporogenesis and all of the mature pollen stage [3]; this is advantageous for a screen of abnormal male meiotic products (in a tetrad) and hence this mutant was used to produce the EMS mutant population mentioned in this paper.

In *Arabidopsis*, errors in DNA repair and recombination, and/or chromosome cohesion and segregation during meiosis, can lead to chromosome fragmentation and to the formation of stretched DNA treads during chromosome segregation [4, 5]. Consequently, plants that are homozygous for mutations responsible for these phenotypes, form abnormal meiotic products due to the uneven segregation of the DNA, giving origin to tetrads with unevenly sized microspores, or to the formation of polyads [4]. This leads to impaired fertility.

Despite the current availability of many tagged (T-DNA and transposon) [6, 7, 8] *Arabidopsis* mutants, there are still a number of genes in *Arabidopsis* that are not annotated in the public databases as being disrupted by T-DNA or transposable elements (www.arabidopsis.org). Moreover, there are plenty of *Arabidopsis* genes that are annotated as having an unknown function (www.arabidopsis.org). Hence, it is possible that some of these genes with no assigned function and/or those for which there are no knock-out mutants available, can have a function in meiosis. Thus, a forward genetics approach is still a valid and unbiased method to identify novel meiotic genes. Consequently, a novel EMS *Arabidopsis* mutant population in a *qrt/qrt* background was produced and screened for meiotic mutants.

Approaches to map EMS mutations have been based on the recombination frequency in the vicinity of the mutation, profiting from the polymorphism between ecotypes (landraces). Gross mapping can map the SNP mutation to a chromosome arm, using a small number of individual plants from a M_2 segregating population [9], while fine mapping usually requires a large amount of M_2 individual plants and big workload. Fortunately, the advent of genomic microarray hybridization for mapping has decreased both the amount of workload as well as the number of M_2 individual plants required for mapping SNP mutations [10].

Materials and Methods

Plant material and EMS mutagenesis

qrt1-1/qrt1-1 mutant seeds (Landsberg *erecta* landrace) (obtained from the *Arabidopsis* stock center) were mutagenized with EMS (Sigma - M0880). The seeds were first submerged in water over night at 4°C. The water was removed and replaced with 0.1% and 0.2% EMS in a 0.1M Na_2HPO_4 (pH 5) solution. The seeds remained in this solution, with agitation at room temperature for 18 hours (0.1% EMS) or eight hours (0.2% EMS). The seeds were washed twice (15 minutes each wash) on a 100mM sodium thiosulphate solution. Several washes with distilled water followed. Finally, the seeds were kept in sterile 0.1% agarose solution for three to four days at 4°C, before being sown in soil; protocol was based on reference [11].

EMS mutant fertility screen

The M_1 plants were grown in soil in a greenhouse, the seeds of each stem being harvested separately (two to three different stems per plant). Seeds from each M_1 stem were grown and the fertility screen was carried out in the M_2 families that segregated sterile or semi-sterile EMS mutant plants. Sterile plants that exhibited gross morphological flower defects or were non-pollinated due to short stamen were not taken into account in the

CBAA - Instituto Superior de Agronomia, Universidade Técnica de Lisboa, Tapada da Ajuda, P-1349-017 Lisboa, Portugal

* Corresponding author. Current address: Disease and Stress Biology Lab - Instituto de Tecnologia Química e Biológica, Universidade Nova de Lisboa, Av. República, Apartado 127, 2781-901 Oeiras, Portugal, Phone: +351 21 4469653, Fax: +351 21 4411277, E-mail: jcnunes@itqb.unl.pt

Q.Y. Shu (ed.), Induced Plant Mutations in the Genomics Era. Food and Agriculture Organization of the United Nations, Rome, 2009, **126-128**

fertility screen. Seeds from individual plants were harvested from the selected M_2 families. All plants were grown in soil.

Cytology screen

The cytology screen was carried out by observing megaspores and microspores using Nomarski optics microscopy [12]. Pictures of microspores and megaspores were taken with a Leica DM LBC microscope and an Evolution MP (media cybernetics) camera. Meiocytes were prepared as described in [13] and the pictures were captured with a U.V. fluorescence microscope U.V. fluorescence Zeiss Axioskop2 microscope and an Axiocam (Zeiss) camera. The images were processed with the Adobe Photoshop 5.0 programme.

Mapping

Fertile M_3 plants (from M_3 families segregating sterile plants) were crossed to Col-0 landrace (obtained from the *Arabidopsis* stock center). The F_1 plants from these crosses were grown, being the F_2 sterile plants used for mapping. All plants were grown in soil. DNA extraction was carried out as described in [14]. Gross mapping was carried out using primers described in [9]. Ongoing mapping using Affymetrix Arabidopsis microarrays was based on [10].

Results

EMS population reveals a Mendelian segregation

For the M_2 *qrt1-1/qrt1-1* EMS mutagenized families so far screened for their fertility, the segregation ratio observed is in agreement with a Mendelian segregation of a single recessive mutant *locus*. Hence, the mutations in these mutants can be attributed to the creation of a single EMS induced SNP per M_2 family, as far as fertility is concerned.

Table 1. Results of the screen carried out to identify M2 impaired fertility mutants affecting meiosis

Number of M_2 families screened for impaired fertility	% of fertility impaired M_2 families	Number of M_2 families submitted to the cytology screen	% of M_2 families segregating meiotic mutant candidates
2500	9.28% (232 / 2500)[a]	110	22.73% (25 / 110)[b]

[a] - (nº of M_2 families segregating fertility impaired plants / total nº of M_2 families screened)
[b] - (nº of M_2 families segregating meiotic mutant candidates / total nº of M_2 families screened in the cytology screen)

Only some (110) out of the 232 M_2 families selected in the impaired fertility screen were subjected to the cytological screen.

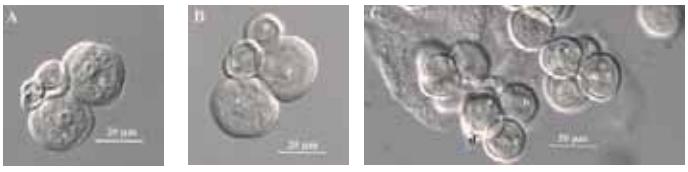

Figure 1 Cytological screen for abnormal haploid spores using Nomarski optics microscopy: Abnormal "tetrads" with unevenly sized microspores (a, b, c, and d) due to an abnormal meiotic division **(A and B)**. Normal tetrads **(C)** with four (a, b, c, d) evenly sized microspores in the *qrt1-1/qrt1-1* mutant genetic background.

Infertility and meiotic screen

While only a fraction of the produced EMS population has so far been screened, 232 candidate M_2 families (out of approximately 2,500) yielded mutants with a sterile or semi-sterile phenotype (**Table 1**). This high number indicates that not all of these mutants are meiotic mutants. Indeed, the cytological screen showed that many are not meiotic mutants since mitotic nuclear divisions in the microspores and megaspores occurred, at least up to a point, as in fertile plants. Mitotic divisions in micro and megaspores occur in the haploid products (spores) of meiosis [15]. Of 110 screened M_2 mutants with impaired fertility, only 25 were selected as being putative meiotic mutant candidates (**Table 1**). The observation of microspore polyads and unevenly sized microspores was a crucial criterion in selecting these 25 candidates (**Fig. 1**). Meiotic chromosome spreading [13] was carried out in 15 of the 25 candidates. Most of the meiotic phenotypes exhibited strong phenotypes of abnormal anaphase I (first meiotic chromosome segregation), where stretched DNA and chromosome fragments were observed. Some examples of the phenotypes observed are shown in **Fig. 2**.

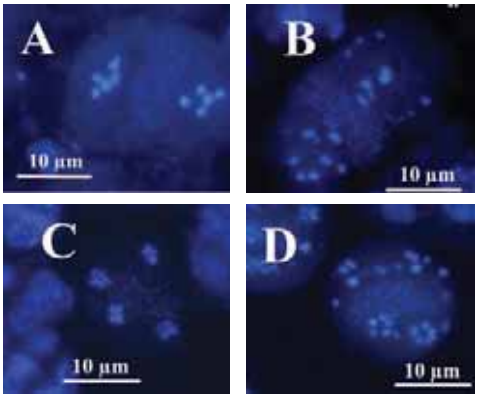

Figure 2 Meiotic stages (DAPI stained) observed in the screened EMS mutants: Normal metaphase II with five chromosomes at each end of the meiotic cell **(A)**. Abnormal metaphase II with unequal number of chromosomes at each end, as well as the presence of small chromosome fragments **(B)**. Normal end product of meiosis (telophase II) with five chromosomes in each of the four meiotic products **(C)**. Abnormal end of meiosis with fragmented chromosomes and chromosome bridges (stretched DNA) **(D)**.

Mapping of the SNP mutant

One of the mutants identified in the screen is now being mapped. Gross mapping [9] revealed that the SNP EMS mutation is located on chromosome III, between the molecular markers nga162 and ciw11.

Microarray hybridization on Affymetrix GeneChip® *Arabidopsis* Tilling 1.0R array is being carried out as in [10]. Wild type Col-0 genomic DNA and pooled genomic DNA of 109 individual sterile EMS mutant plants are being used in these hybridizations.

Discussion

This forward genetics approach using a EMS mutant population will allow an unbiased screen (not based on homologies to known genes) which could lead to the discovery of yet unknown and/or plant-specific meiotic genes. Furthermore, by combining three different screens, this approach has the advantage of eliminating most of the non-meiotic sterile mutant candidates at the second screen (by observing the microspores and megaspores of non-fertile plants, see **Fig. 1**). Consequently, a large number of the sterile plants screened after the 2nd screen were indeed shown to be sterile due to abnormal meiotic division, mainly during the first meiotic division.. Most of the observed mutations manifested themselves during the first meiotic division, probably due to a defective recombination apparatus, or due to an inefficient release of chromosome cohesion (see **Fig. 2**).

Despite this three-steps screen being a very efficient way of selecting meiotic mutants, it is still labor- intensive and time-consuming. Yet, the combined gross mapping and the Affymetrix GeneChip® Arabidopsis Tiling 1.0R array hybridization based mapping (ongoing) are expected to reduce significantly the time and labor invested in mapping.

This three-steps screen combined with a more efficient mapping approach, and complemented with allele tests, should lead to the identification of novel meiotic *Arabidopsis* genes.

ACKNOWLEDGEMENTS

J.A. da C-N designed the experiments, carried out the work, and wrote the paper. He was supported by F.C.T. (Fundação para a Ciência e Tecnologia), fellowships (SFRH/BPD/30365/2006) and (SFRH/BPD/7137/2001), and is thankful to W.V. who provided the facilities to carry out the work. The W.V. lab is funded by the F.C.T., Portugal. J.A. da C.-N also thanks I.G.C. (Instituto Gulbenkian de Ciência, Portugal) for granting access to microscopes.

BIBLIOGRAPHY

1. Hamant, O., Ma, H., Cande, W.Z. Genetics of meiotic prophase I in plants. *Annual Review In Plant Biology* **57**, 267-302 (2006).

2. Ross, K.J., Fransz, P., Jones, G.H. A light microscopic atlas of meiosis in Arabidopsis thaliana. *Chromosome Research* **4**, 507-516 (1996).

3. Preuss, D., Rhee, S.Y., Davis, R.W. Tetrad analysis possible in Arabidopsis with mutation of the QUARTET (QRT) genes. *Science* **264**, 1458-1460 (1994).

4. Bhatt, A.M., Lister, C., Page, T., Fransz, P., Finddlay, K., Jones, G.H., Dickinson, H.G., Dean, C. The *DIF1* gene of *Arabidopsis* is required for meiotic chromosome segregation and belongs to the *REC8/RAD21* cohesin gene family. *The Plant Journal* **19**, 463-472 (1999).

5. Bleuyard, J.-Y., Gallego, M.G., Savigny, F., White, C.I. Differing requirements for the *Arabidopsis* Rad51 paralogs in meiosis and DNA repair. *The Plant Journal* **41**, 533-545 (2005).

6. Sessions, A., Burke, E., Presting, G., Aux, G., Mcelver, J., Patton, D., Dietrich, B., Ho, P., Bacwaden, J., Ko, C., Clarke, J.D., Coton, D., Bullis, D., Snell, J., Miguel, T., Hutchison, D., Kimmerly, B., Mitzel, T., Katagiri, F., Glazebrook, J., Law, M., Goff, S.A. A high-throughput *Arabidopsis* reverse genetics system. *Plant Cell* **14**, 2985-94 (2002).

7. Alonso, J.M., Stepanova, A.N., Leisse, T.J., Kim, C.J., Chen, H., Shinn, P., Stevenson, D.K., Zimmerman, J., Barajas, P., Cheuk, R., Gadrinab, C., Heller, C., Jeske, A., Koesema, E., Meyers, C.C., Parker, H., Prednis, L., Ansari, Y., Choy, N., Deen, H., Geralt, M., Hazari, N., Hom, E., Karnes, M., Mulholland, C., Ndubaku, R., Schmidt, I., Guzman, P., Aguilar-Henonin, L., Schmid, M., Weigel, D., Carter, D.E., Marchand, T., Risseeuw, E., Brogden, D., Zeko, A., Crosby, W.L., Berry, C.C., Ecker, J.R. Genome-Wide Insertional Mutagenesis of *Arabidopsis thaliana*. *Science* **301**, 653-657 (2003).

8. Rosso, M.G., Li, Y., Strizhov, N., Reiss, B., Dekker, K., Weisshaar, B. An *Arabidopsis thaliana* T-DNA mutagenized population (GABI-Kat) for flanking sequence tag-based reverse genetics. *Plant Molecular Biology* **53**, 247-259 (2003).

9. Lukowitz, W., Gillmor, C.S., Scheible, W.-R. Positional cloning in *Arabidopsis*. Why it feels good to have a genome initiative working for you. *Plant Physiology* **123**, 795-805(2000).

10. Hazen, S.P., Borevitz, J.O., Harmon, F.G., Pruneda-Paz, J.L., Schultz, T.F., Yanovsky, M.J., Liljegren, S.J., Ecker, J.R., Kay, S.A. Rapid array mapping of circadian clock and developmental mutations in *Arabidopsis*. *Plant Physiology* **138**, 990-997 (2005).

11. Jander, G., Baerson, S.R., Hudak, J.A., Gonzalez, K.A., Gruys, K.J., Last, R.L. Ethylmethanesulfonate saturation mutagenesis in *Arabidopsis* to determine frequency of herbicide resistance. *Plant Physiology* **131**, 139-146 (2003).

12. Yadegari, R., De Paiva, G.R., Laux, T., Koltunow, A.M., Apuya, N., Zimmerman, J.L., Fischer, R.L., Harada, J.J., Goldberg, R.B. Cell differentiation and morphogenesis are uncoupled in *Arabidopsis raspberry* embryos. *The Plant Cell* **6**, 1713-1729 (1994).

13. Armstrong, S.J., Franklin, F.C.H., Jones, G.H. Nucleolus-associated Telomere clustering and pairing precede meiotic chromosome synapsis in *Arabidopsis thaliana*. *Journal Of Cell Science* **114**, 4207-4217 (2001).

14. Edwards, K., Johnstone, C., Thompson, C. A simple and rapid method for the preparation of plant genomic DNA for PCR analysis. *Nucleic Acids Research* **19**, 1349 (1991).

15. Da Costa-Nunes, J.A., Grossniklaus, U. Unveiling the gene-expression profile of pollen. *Genome Biology* **5**, 205.1-205.3 (2003).